Journal of Materials Chemistry C

ROYAL SOCIETY OF CHEMISTRY

PAPER

View Article Online
View Journal | View Issue



Cite this: J. Mater. Chem. C, 2020, 8, 12470

# Spiro-type host materials with rigidified skeletons for RGB phosphorescent OLEDs†

Aziz Khan,‡ Xing Chen,‡ Sarvendra Kumar, Sheng-Yi Yang, You-Jun Yu, Wei Luo, Zuo-Quan Jiang,* Man-Keung Fung* and Liang-Sheng Liao

Received 18th March 2020,
Accepted 1st August 2020

DOI: 10.1039/d0tc01389g

rsc.li/materials-c

A universal host material for red, green and blue phosphors raises challenges for the fabrication of efficient phosphorescent organic light-emitting diodes (PHOLEDs). Herein, two spiro host materials, namely 3-(4,6-diphenyl-1,3,5-triazin-2-yl)-9′,9′-dimethyl-9′*H*-spiro[fluorene-9,5′-quinolino[3,2,1-de]acridine] (**QAF-TRZ**) and 3′-(4,6-diphenyl-1,3,5-triazin-2-yl)-10-phenyl-10*H*-spiro[acridine-9,9′-fluorene] (**STF-TRZ**), are designed and synthesized. The designed strategy is more appropriate and rarely found among the reported spiro-based skeletons for organic light-emitting diodes (OLEDs). Both materials exhibited excellent electroluminescence performance. In particular, the RGB three-color PHOLEDs based on **QAF-TRZ** and **STF-TRZ** as hosts and FIrpic, $Ir(ppy)_2acac$, and $Ir(MDQ)_2acac$ as emitters are fabricated. The blue PHOLEDs based on **QAF-TRZ** realize a maximum external quantum efficiency (EQE) of 19.4%, and remain 17.2% at 1000 cd $m^{-2}$. On the other hand, green PHOLEDs show maximum EQEs of 21% and 19% for **QAF-TRZ** and **STF-TRZ**, respectively, and both devices exhibit low efficiency roll-off. The red devices obtain EQEs of 22.6% and 19.4% based on **QAF-TRZ** and **STF-TRZ**, respectively, in which the former has among the most efficient value. Consequently, these results confirm that host materials incorporating the spiro-motif with sufficiently high triplet energy are promising for obtaining high performance RGB-based PHOLEDs. The better device performance based on **QAF-TRZ** stems from its better hole transport capability, resulting in a superior charge recombination efficiency.



## Introduction

Organic light-emitting diodes (OLEDs) have attracted widespread interest in both academia and industry, because of the fascinating applications in flat panel displays and solid-state lighting.[1–5] Generally, in fluorescent OLEDs the non-radiative process limits the internal quantum efficiency (IQE) to 25% while the external quantum efficiency (EQE) hardly exceeds 5%.[6] To resolve this issue, Forrest *et al.* reported phosphorescent organic light-emitting diodes (PHOLEDs) containing platinum(II) or iridium(III) complexes, which could successfully obtain 100% IQE *via* spin–orbit coupling, utilizing both singlet and triplet excitons.[7–11] Since then, many efforts have been made to improve device performance and stability. On the other hand, phosphorescent OLEDs doped into a host material is also highly critical to mitigate triplet–triplet annihilation and concentration quenching phenomena.[12,13] Host materials usually have two design strategies. Firstly, to prevent the reverse energy transfer from guest to host, the host materials must have a higher triplet energy level ($E_T$) than the guest. Secondly, to reduce the turn-on voltage and facilitate effective injection of hole and electron, appropriate levels of the highest occupied molecular orbitals (HOMOs) and the lowest unoccupied molecular orbitals (LUMOs) of the host to adjacent material layers are highly required.[14–19]

Compared with unipolar hosts,[20,21] bipolar host materials attract more attention because both the hole and electron transport elements can be found in a single molecule.[22–27] In this regard, many groups have strived to design bipolar host materials with good efficiency.[7,22,23,28] Among them, spiro-type[29–36] bipolar hosts are of particular interest due to the following features: (i) the 3-D configuration can enhance the thermal and morphological stabilities, (ii) the functionalization of spiro-hosts is flexible, *i.e.* chemists have the flexibility to modify not only the acceptor unit but also the donor unit of the hemisphere, (iii) this modification can balance hole/electron transport. In designing bipolar compounds in the most classic 9,9′-spirobifluorene, many electron-rich spiro backbones have been developed with an appended electron acceptor (Scheme 1a).

Herein, two novel spiro-type bipolar host materials, namely 3-(4,6-diphenyl-1,3,5-triazin-2-yl)-9′,9′-dimethyl-9′*H*-spiro[fluorene-9,5′-quinolino[3,2,1-de]acridine] (**QAF-TRZ**) and 3′-(4,6-diphenyl-1,3,5-triazin-2-yl)-10-phenyl-10*H*-spiro[acridine-9,9′-fluorene]

*Institute of Functional Nano & Soft Materials (FUNSOM), Jiangsu Key Laboratory for Carbon-Based Functional Materials & Devices, Soochow University, 199 Ren'ai Road, Suzhou, 215123, Jiangsu, P. R. China.*
*E-mail: zqjiang@suda.edu.cn, mkfung@suda.edu.cn*

† Electronic supplementary information (ESI) available. See DOI: 10.1039/d0tc01389g

‡ These authors contributed equally to this work.

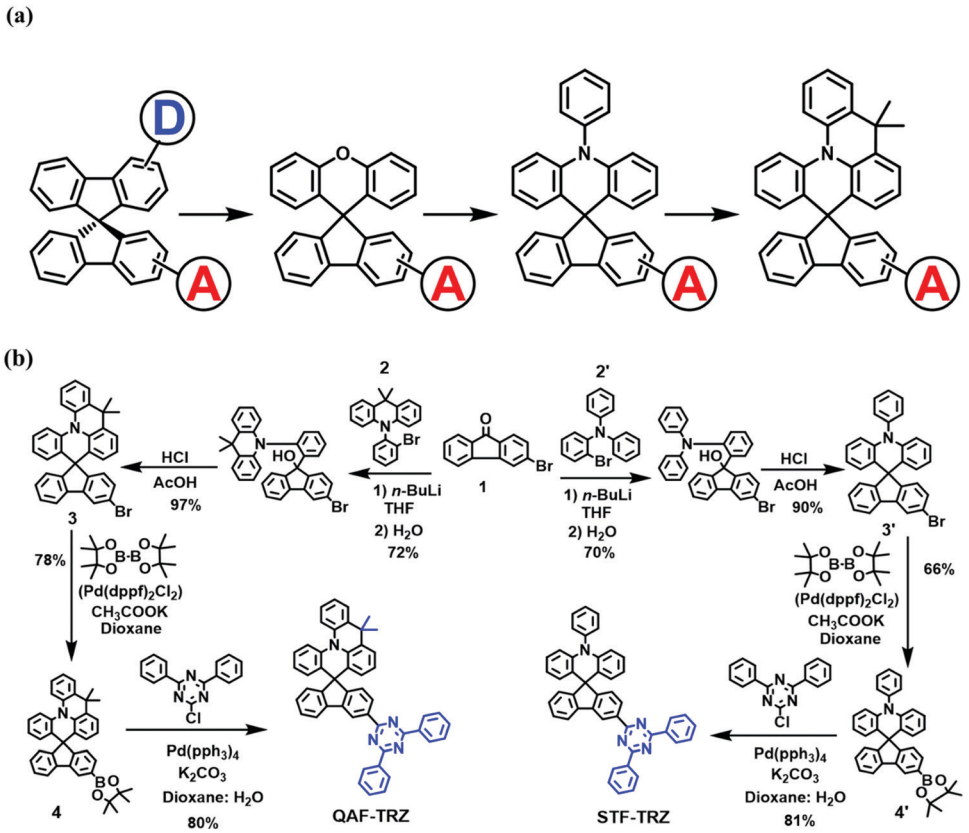


Scheme 1 (a) The derivatization of donor/acceptor host materials in the spiro-skeleton. (b) The synthetic routes for **QAF-TRZ** and **STF-TRZ**.

(**STF-TRZ**), containing 9,9-dimethyl-10-phenyl-9,10-dihydroacridine and a triphenylamine donor linking with a strong triazine acceptor through the spiro bridge are prepared, respectively. In comparison, **QAF-TRZ** with the new rigidified donor moiety has a prominent effect on the photophysical and thermal properties and electroluminescence (EL) device performance. We systematically investigated both materials as universal hosts in blue/green/red PHOLEDs. As a result, the devices based on **QAF-TRZ** show superior performances and lower efficiency roll-off than **STF-TRZ**, demonstrating the potential of this new spiro-structure as a PHOLED host.

## Experimental section

Compound **1** and **2′** were purchased while compound **2** was synthesized according to prior literature.[37,38]

### 3-Bromo-9′,9′-dimethyl-9′*H*-spiro[fluorene-9,5′-quinolino-[3,2,1-de]acridine] (3)

The compound **2**, (10-(2-bromophenyl)-9,9-dimethyl-9,10-dihydroacridine) (2.0 g, 5.6 mmol) was dissolved in THF (40 mL) under an inert environment. The *n*-butyl lithium (1.6 M solution in hexane 2.2 mL, 5.5 mmol) was added slowly at −78 °C, and the reaction mixture was stirred for 1 hour at the same condition. Then, THF solution (20 mL) of 3-bromo-9*H*-fluoren-9-one (1.1 g, 4.6 mmol) was added and further stirred for 2 hours at −78 °C. It was then stirred overnight at room temperature. After completion, the reaction mixture was quenched with water (5 mL). The THF was evaporated and the obtained viscous solid was extracted with dichloromethane (DCM) and washed with water (30 mL × 3). The organic portion was collected and purified through column until white solid, about 1.8 g (72%), was obtained, which was used in the next reaction after purification. The intermediate 3-bromo-9-(2-(9,9-dimethylacridin-10(9*H*)-yl)phenyl)-9*H*-fluoren-9-ol was dissolved in acetic acid (30 mL) refluxed at 80 °C for 20 minutes. Then, hydrochloric acid (8 mL) was added slowly to the reaction mixture. After 4 hours, a white solid appeared. It was filtered off and washed first with water and then petroleum ether (PE). Column chromatography was used for further purification: PE/DCM (7/3, v/v) (1.6 g, 97%). $^1$H NMR (400 MHz, $CDCl_3$) $\delta$ (ppm) 8.05 (d, $J$ = 1.8 Hz, 1H), 7.88 (d, $J$ = 7.6 Hz, 1H), 7.83 (d, $J$ = 1.7 Hz, 1H), 7.72 (dd, $J$ = 12.3, 4.3 Hz, 1H), 7.67 (d, $J$ = 7.9 Hz, 1H), 7.60 (ddd, $J$ = 8.1, 6.1, 1.5 Hz, 2H), 7.54–7.46 (m, 1H), 7.39–7.30 (m, 2H), 7.27–7.18 (m, 2H), 7.13 (d, $J$ = 7.7 Hz, 1H), 7.07 (dd, $J$ = 8.2, 1.8 Hz, 1H), 7.02–6.94 (m, 1H), 6.85 (td, $J$ = 7.6, 3.0 Hz, 2H), 6.65 (ddd, $J$ = 9.6, 7.9, 1.4 Hz, 1H), 6.45 (ddd, $J$ = 9.0, 7.8, 1.2 Hz, 1H), 1.99 (s, 3H), 1.39 (s, 3H). $^{13}$C NMR (100 MHz, $CDCl_3$) $\delta$ (ppm) 154.60, 152.92, 150.51, 149.26, 144.90, 141.43, 139.18, 138.61, 136.98, 136.35, 135.57, 134.29, 131.71, 131.01, 129.11, 128.68, 128.42, 127.40, 126.79, 126.59, 125.41, 124.47, 124.03, 123.71, 123.61, 123.04, 122.51, 121.40, 120.37, 118.50, 116.91, 57.36, 36.93, 31.81, 23.02. MS (EI) $m/z$: 525.08 [$M^+$].

### 3′-Bromo-10-phenyl-10*H*-spiro[acridine-9,9′-fluorene] (3′)

The intermediate **3′** was synthesized according to the similar procedure as explained above for compound **3** except by changing the corresponding reagents. It was further purified using column chromatography with eluents: PE/DCM (8/2, v/v) (1.3 g, 90%). $^1$H NMR (400 MHz, $CDCl_3$ $\delta$ (ppm) 7.97 (d, $J$ = 1.7 Hz, 1H), 7.83–7.71 (m, 3H), 7.62 (t, $J$ = 7.5 Hz, 1H), 7.53 (d, $J$ = 8.4 Hz, 2H), 7.50–7.39 (m, 3H), 7.32 (dd, $J$ = 18.3, 9.5 Hz, 2H), 7.01–6.92 (m, 2H), 6.62 (t, $J$ = 7.5 Hz, 2H), 6.42 (dd, $J$ = 16.2, 8.5 Hz, 4H). $^{13}$C NMR (100 MHz, $CDCl_3$) $\delta$ (ppm) 156.81, 155.39, 141.34, 140.96, 137.93, 131.16, 129.17, 128.56, 127.74, 127.38, 125.97, 124.01, 123.17, 121.69, 120.65, 120.17, 114.79, 56.66. MS (EI) $m/z$: 485.24 [$M^+$].

### 9′,9′-Dimethyl-3-(4,4,5,5-tetramethyl-1,3,2-dioxaborolan-2-yl)-9′*H*-spiro[fluorene-9,5′-quinolino[3,2,1-de]acridine] (4)

A mixture of 3-bromo-9′,9′-dimethyl-9′*H*-spiro[fluorene-9,5′-quinolino[3,2,1-de]acridine] (1.3 g, 2.4 mmol), 4,4,40,40,5,5,50,50-octamethyl-2,20-bi(1,3,2-dioxaborolane) (1.2 g, 4.9 mmol), 1,1′-bis(diphenylphosphino)ferrocene-palladium(II) ($Pd(dppf)_2Cl_2$) 87.0 mg, 0.1 mmol), potassium acetate (1.1 g, 12.0 mmol), and anhydrous 1,4-dioxane (50 mL) was degassed and then refluxed under an inert atmosphere for 24 hours at 80 °C. The reaction mixture was washed three times with water (30 mL × 3) after dilution with DCM. In order to remove water completely from the organic part, anhydrous $MgSO_4$ was added. The solvent of crude product was dried through a rotary evaporator, which was purified using column chromatography to obtain a white powder with the eluents: PE/DCM (4/6, v/v) (1.1 g, 78%). $^1$H NMR (400 MHz, $CDCl_3$) $\delta$ (ppm) 8.37 (s, 1H), 8.17 (s, 1H), 7.96 (dd, $J$ = 14.1, 7.5 Hz, 1H), 7.80–7.69 (m, 1H), 7.68–7.54 (m, 2H), 7.53–7.42 (m, 2H), 7.38–7.29 (m, 2H), 7.18 (ddd, $J$ = 23.6, 14.6, 8.3 Hz, 3H), 6.94 (t, $J$ = 7.5 Hz, 1H), 6.82 (dd, $J$ = 9.2, 4.6 Hz, 2H), 6.67–6.60 (m, 1H), 6.44 (t, $J$ = 7.2 Hz, 1H), 1.98 (s, 3H), 1.47 (s, 6H), 1.39 (s, 3H), 1.32 (s, 6H).$^{13}$C NMR (100 MHz, $CDCl_3$) $\delta$ (ppm) 153.73, 149.96, 139.28, 138.62, 136.99, 136.41, 135.24, 134.68, 134.19, 134.14, 129.23, 128.24, 128.06, 127.42, 127.13, 127.06, 126.90, 126.67, 126.46, 126.37, 124.39, 123.98, 123.85, 123.27, 123.02, 122.86, 122.11, 120.38, 120.34, 118.42, 118.38, 116.98, 116.92, 84.05, 83.72, 57.68, 36.92, 31.77, 31.66, 25.00, 24.83, 24.79, 23.02. MS (EI) $m/z$: 573.29 [$M^+$].

### 10-Phenyl-3′-(4,4,5,5-tetramethyl-1,3,2-dioxaborolan-2-yl)-10*H*-spiro[acridine-9,9′ fluorene] (4′)

The compound **4′** was synthesized according to the similar procedure mentioned above for compound **4** only by changing the corresponding reagents. In order to obtain pure product, it was passed through column chromatography with the eluents: PE/DCM (4/6, v/v) (0.8 g, 66%). $^1$H NMR (400 MHz, $CDCl_3$) $\delta$ (ppm) 8.30 (s, 1H), 7.88 (d, $J$ = 7.5 Hz, 1H), 7.81–7.69 (m, 3H), 7.60 (t, $J$ = 8.0 Hz, 1H), 7.53 (d, $J$ = 8.1 Hz, 2H), 7.46 (dd, $J$ = 14.3, 7.5 Hz, 2H), 7.39 (t, $J$ = 8.0 Hz, 1H), 7.25 (d, $J$ = 7.4 Hz, 1H), 6.97–6.89 (m, 2H), 6.57 (t, $J$ = 7.5 Hz, 2H), 6.39 (dd, $J$ = 13.7, 7.3 Hz, 4H), 1.42 (s, 12H). $^{13}$C NMR (100 MHz, $CDCl_3$) $\delta$ (ppm) 159.53, 156.68, 141.17, 138.95, 135.10, 131.15, 128.40, 127.87, 127.58, 127.21, 126.33, 125.66, 125.35, 124.54, 120.54, 120.18, 114.63, 83.90, 56.97, 24.94. MS (EI) $m/z$: 533.35 [$M^+$].

### 3-(4,6-Diphenyl-1,3,5-triazin-2-yl)-9′,9′-dimethyl-9′*H*-spiro-[fluorene-9,5′-quinolino[3,2,1-de]acridine] (QAF-TRZ)

The compounds 9′,9′-dimethyl-3-(4,4,5,5-tetramethyl-1,3,2-dioxaborolan-2-yl)-9′*H*-spiro[fluorene-9,5′quinolino[3,2,1-de] acridine] (0.8 g,1.5 mmol), 2-chloro-4,6-diphenyl-1,3,5 triazine (0.5 g, 1.8 mmol), tetrakis(triphenylphosphine)palladium(0) (50.0 mg, 0.05 mmol) and potassium carbonate (0.5 g, 3.7 mmol) were dissolved in 1,4-dioxane/$H_2O$ (40 : 4), and refluxed for 24 hours at 85 °C. The mixture was diluted with DCM and washed thrice with distilled water (100 mL). The organic layer was dried and purified through column chromatography using PE/DCM (7/3, v/v) to obtain a pale white powder (0.8 g, 80%). $^1$H NMR (600 MHz, $CDCl_3$) $\delta$ (ppm) 9.25 (s, 1H), 9.02 (s, 1H), 8.87 (dd, $J$ = 14.1, 7.3 Hz, 2H), 8.73 (d, $J$ = 7.1 Hz, 2H), 8.36 (d, $J$ = 8.1 Hz, 1H), 8.14 (d, $J$ = 7.6 Hz, 1H), 7.93 (d, $J$ = 7.5 Hz, 1H), 7.79 (d, $J$ = 8.0 Hz, 1H), 7.73 (d, $J$ = 8.0 Hz, 1H), 7.70–7.48 (m, 8H), 7.36 (s, 1H), 7.31 (t, $J$ = 7.2 Hz, 1H), 7.20 (t, $J$ = 8.9 Hz, 1H), 7.15 (d, $J$ = 7.6 Hz, 1H), 6.98 (t, $J$ = 7.5 Hz, 1H), 6.83 (dd, $J$ = 13.1, 7.2 Hz, 2H), 6.69 (dd, $J$ = 14.3, 7.9 Hz, 1H), 6.49 (dd, $J$ = 18.7, 7.8 Hz, 1H), 1.97 (s, 3H), 1.39 (s, 3H). $^{13}$C NMR (150 MHz, $CDCl_3$) $\delta$ (ppm) 171.73, 158.31, 155.01, 154.51, 150.38, 143.51, 142.24, 139.26, 138.69, 137.70, 137.03, 136.67, 136.16, 135.75, 134.32, 132.58, 131.96, 129.64, 129.42, 127.81, 127.04, 126.63, 124.51, 124.31, 123.39, 123.08, 122.39, 120.95, 118.56, 117.02, 57.79, 36.98, 31.84, 23.08. MALDI-TOF ($m/z$) calculated for $C_{49}H_{34}N_4$ [$M^+$]: 678.27, found: 678.22. Anal. calcd for $C_{49}H_{34}N_4$ C, 86.70; H, 5.05: N, 8.25 found C, 85.92; H, 4.97: N, 8.07.

### 3′-(4,6-Diphenyl-1,3,5-triazin-2-yl)-10-phenyl-10H-spiro-[acridine-9,9′-fluorene] (STF-TRZ)

A mixture of 10-phenyl-3′-(4,4,5,5-tetramethyl-1,3,2-dioxaborolan-2-yl)-10*H*-spiro[acridine-9,9′-fluorene] (0.7 g, 1.3 mmol), 2-chloro-4,6-diphenyl-1,3,5 triazine (0.4 g, 1.6 mmol), tetrakis (triphenylphosphine) palladium (0) (50.0 mg, 0.04 mmol) and potassium carbonate (0.4 g, 3.2 mmol) was dissolved in 1,4-dioxane/$H_2O$ (40 : 4) refluxed over night at 85 °C. The crude organic layer was subjected to column chromatography for further purification using PE/DCM (7/3, v/v) (0.68 g, 81%). $^1$H NMR (600 MHz, $CDCl_3$) $\delta$ (ppm) 9.15 (s, 1H), 8.81 (d, $J$ = 6.9 Hz, 4H), 8.69 (d, $J$ = 8.0 Hz, 1H), 8.05 (d, $J$ = 7.5 Hz, 1H), 7.73 (t, $J$ = 7.6 Hz, 2H), 7.68–7.56 (m, 8H), 7.54 (d, $J$ = 7.8 Hz, 2H), 7.47 (dd, $J$ = 17.7, 10.3 Hz, 2H), 7.33 (t, $J$ = 7.4 Hz, 1H), 6.94 (t, $J$ = 7.7 Hz, 2H), 6.58 (t, $J$ = 7.4 Hz, 2H), 6.47 (d, $J$ = 6.9 Hz, 2H), 6.39 (d, $J$ = 8.4 Hz, 2H). $^{13}$C NMR (150 MHz, $CDCl_3$) $\delta$ (ppm) 171.83, 171.64, 160.63, 156.52, 141.28, 140.99, 139.87, 138.70, 136.25, 135.95, 132.51, 131.17, 131.08, 129.54, 128.97, 128.84, 128.65, 128.49, 127.77, 127.74, 127.39, 125.96, 125.87, 124.25, 120.63, 120.53, 120.40, 114.73, 57.03. MALDI-TOF ($m/z$) calculated for $C_{46}H_{30}N_4$ [$M^+$]: 638.24, found: 638.18. Anal. calcd for $C_{46}H_{30}N_4$ C, 86.49; H, 4.73: N, 8.77 found C, 85.58; H, 4.69: N, 8.39.

## Results and discussion

### Synthesis and characterization

The synthetic routes for two compounds are depicted in Scheme 1b. The intermediate **3** and **3′** were synthesized through a three-step

 

consecutive reaction under the same conditions. Similarly, the intermediate **4** and **4′** were synthesized through the Miyaura borylation reaction.[39] Finally, **QAF-TRZ** and **STF-TRZ** were successfully obtained in good yields through the Suzuki–Miyaura coupling reaction with 2-chloro-4,6-diphenyl-1,3,5 triazine and corresponding reagents **4** and **4′**. To make it highly pure, the products were further sublimated under vacuum after column chromatography before being used in OLED devices. The chemical structures of **QAF-TRZ** and **STF-TRZ** were fully characterized through $^{1}$H and $^{13}$C NMR spectroscopy, mass spectrometry, and elemental analysis.

### Thermal properties

The thermogravimetric analysis (TGA) and differential scanning calorimetry (DSC) under inert atmosphere are shown in Fig. S1a and b (ESI†) for both compounds. The measured thermal properties and values are depicted in Table 1. The spiro annulated structure reveals high decomposition temperatures ($T_d$) with 5% weight loss observed at 430 and 424 °C, while the glass transition temperatures ($T_g$) are 195 and 158 °C for **QAF-TRZ** and **STF-TRZ**, respectively. Comparably, **QAF-TRZ** has more favorable $T_d$ and $T_g$ over the **STF-TRZ** for OLED preparation in vacuum deposition due to the rigidification in the spiro-skeleton.

### Theoretical calculations

Theoretical calculations were performed to better understand the electronic properties of the two compounds by using density functional theory (DFT) and time-dependent DFT (TD-DFT). Ground-state geometries and excited state geometries were optimized at the B3LYP/6-31G level.[40] The highest occupied molecular orbital (HOMO) and the lowest unoccupied molecular orbital (LUMO) of **QAF-TRZ** and **STF-TRZ** are mainly located at the donor and acceptor segment, respectively (Fig. 1a). The energy level of the HOMO and LUMO of **QAF-TRZ** and **STF-TRZ** are −5.04/−1.90 eV and −5.00/−1.74 eV, respectively (Fig. 1b); the fused strategy on the donor leads to a deeper HOMO and higher singlet/triplet energies as unveiled from the photophysical measurements (*vide infra*). Furthermore, the energy differences between the $S_1$ and $T_1$ states for **QAF-TRZ** and **STF-TRZ** are almost the same. Based on the electron–hole distribution analysis,[41] 99.2% and 99.3% of the HOMO-to-LUMO transitions contributed to the S0 → S1 excitation for **QAF-TRZ** and **STF-TRZ**, respectively, while contributions to the S0 → T1 excitation was 98.0% and 96.7%, respectively, for **QAF-TRZ** and **STF-TRZ**.

Table 1 Summary of the physical properties of **QAF-TRZ** and **STF-TRZ**

| Compounds | $^{Abs}$[a] (nm) | $^{Fl}$[b] (nm) | $^{Phos}$[c] (nm) | $E_g$[d] (eV) | $E_T$[e] (eV) | HOMO/LUMO[f] (eV) | $T_d/T_g$[g] (°C) |
|---|---|---|---|---|---|---|---|
| **QAF-TRZ** | 305 | 447 | 447 | 3.44 | 2.88 | −5.67/−2.23 | 430/195 |
| **STF-TRZ** | 305 | 450 | 446 | 3.44 | 2.86 | −5.36/−1.91 | 424/158 |

[a] Calculated from the UV-vis absorption measured in toluene. [b] Determined from the room temperature fluorescence in toluene. [c] Calculated from the 77 K phosphorescence in toluene. [d] Calculated from the UV-vis absorption in toluene. [e] Calculated from the phosphorescence in toluene. [f] HOMO is calculated from the oxidation potential with respect to reference ferrocene; LUMO is calculated from the energy gap plus HOMO. [g] $T_d$: decomposition temperature, $T_g$: glass transition temperature.

### Photophysical properties

The photophysical behavior of **QAF-TRZ** and **STF-TRZ** was recorded using ultraviolet-visible (UV-vis) and fluorescence spectroscopy in toluene at room temperature. Phosphorescence spectra were measured at frozen temperature (77 K) using the same solvent and are depicted in Fig. 2a and b, respectively. **QAF-TRZ** and **STF-TRZ** show very similar absorption peaks at 305 nm, which is attributed to the π–π* transitions. The HOMO–LUMO energy gaps were calculated from the UV absorption onset, and both are 3.44 eV. The fluorescence peaks as observed in the photoluminescence spectra (PL) for **QAF-TRZ** and **STF-TRZ** were 447 and 450 nm, respectively. Apart from that, the photophysical properties of **QAF-TRZ** and **STF-TRZ** were also measured in neat film and their spectra are illustrated in Fig. S2 (ESI†). Notably, the absoption peak for **QAF-TRZ** and **STF-TRZ** is blue-shifted as compared to that of the solution results; the triplet-energy levels for **QAF-TRZ** and **STF-TRZ** are quite similar as well. Moreover, the triplet energies calculated from the vibronic band of the phosphorescence spectra at 77 K are 2.88 eV for **QAF-TRZ**, and 2.86 eV for **STF-TRZ**. Therefore, such triplet energies are high enough to prevent back energy transfer from emitters.

### Electrochemical properties

To investigate the electrochemical behavior of the two host materials, **QAF-TRZ** and **STF-TRZ**, cyclic voltammetry analysis was performed in anhydrous DCM using ferrocene as the internal standard and the parameters are summarized in Table 1. The oxidation potential values for the compounds **QAF-TRZ** and **STF-TRZ** are +1.37 V and +1.05 V, respectively. The obtained results indicate that **QAF-TRZ** is constructed with a rigid donor structure as compared to **STF-TRZ**. The HOMO energy levels were estimated from the onset of the oxidation potential curves to be −5.67/−5.36 eV, respectively, while the LUMO energy levels were calculated from $E_g$ (onset of UV-vis spectra) and HOMO values, which were −2.23/−1.91 eV for **QAF-TRZ** and **STF-TRZ**, respectively (Fig. S3, ESI†).

### Electroluminescence (EL) properties

To further evaluate the EL properties of these two host materials, we first fabricated blue PHOLED devices based on **FIrpic**. As shown in Fig. 3a, the blue device structure is ITO/1,4,5,8,9,11-hexaazatriphenylene-hexacarbonitrile (HAT-CN) (10 nm)/1,1-bis[4-[*N*,*N*-di(*p*-tolyl)amino]phenyl]cyclohexane (TAPC) (40 nm)/tris (4-(9*H*-carbazol-9-yl)phenyl)amine (TCTA) (10 nm)/**QAF-TRZ** or **STF-TRZ**:**FIrpic** 15 wt% (20 nm)/3,3′-(5′-(3-(pyridin-3-yl)phenyl)-[1,1′:3′,1″-terphenyl]-3,3″-diyl)dipyridine (TmPyPB) (45 nm)/(8-quinolinolato lithium) Liq (2 nm)/Al (100 nm) (**B1** for **QAF-TRZ** and **B2** for **STF-TRZ**). The energy level diagrams of all the blue, green and red devices fabricated in the present studies are displayed in Fig. 3b. ITO acts as the anode while Al acts as the cathode. HAT-CN and Liq are the hole and electron-injection

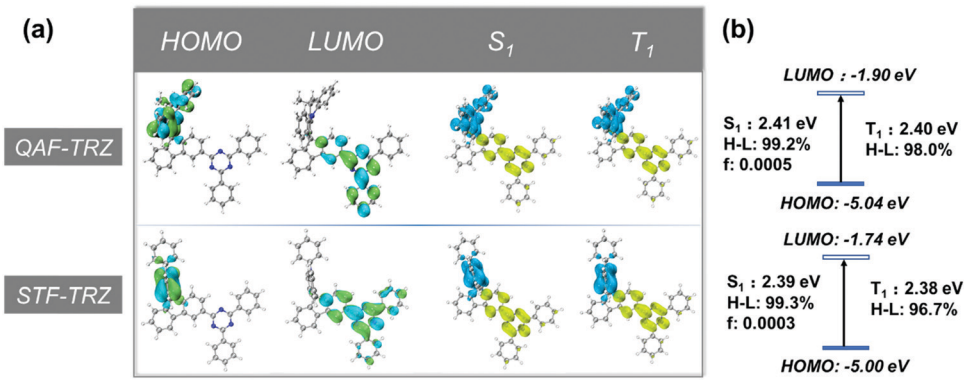


Fig. 1 (a) The distribution of HOMOs and LUMOs and the analysis for distribution of hole (blue), electron (yellow) for $S_1$ and $T_1$ and (b) energy level diagram of HOMOs, LUMOs, $S_1$ and $T_1$.

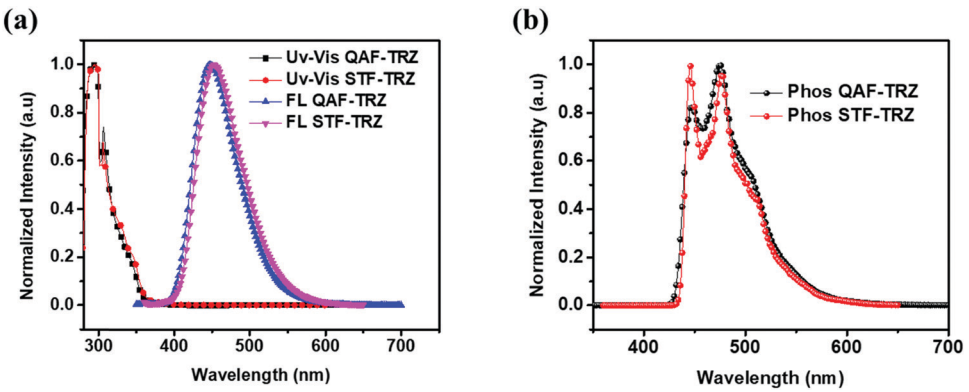


Fig. 2 (a) Normalized UV-vis absorption and fluorescence emission spectra in toluene at room temperature. (b) Phosphorescence spectra in frozen toluene at 77 K for compounds **QAF-TRZ** and **STF-TRZ**.

layers, respectively. TAPC is employed as the hole transport layer because of its remarkable hole mobility and TCTA plays the role of the electron blocking layer. Furthermore, TmPyPB is chosen as the electron transport layer for better energy level

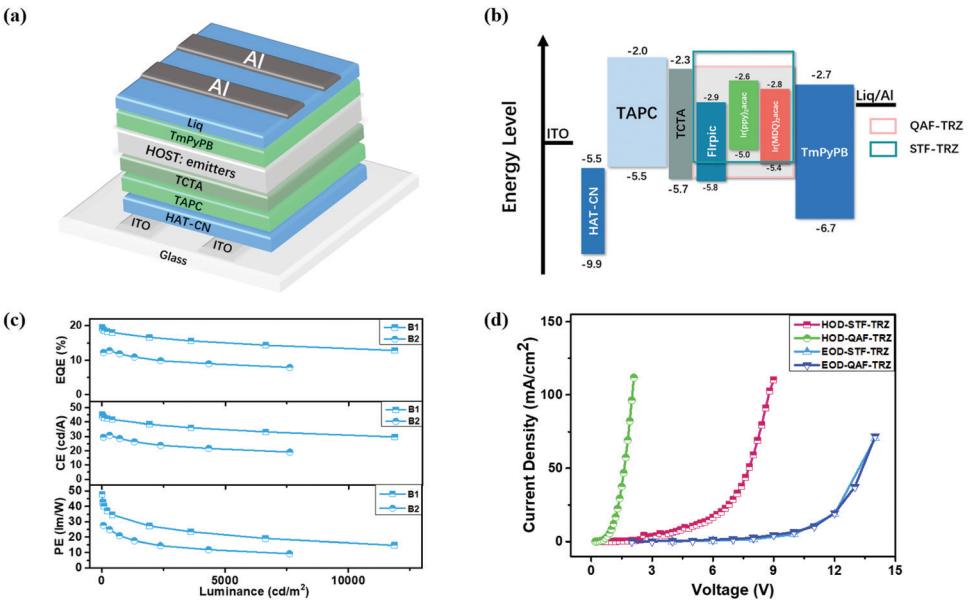


Fig. 3 (a) Device structure, (b) energy level diagrams of devices, (c) blue PHOLED performance and (d) hole-only and electron-only devices based on **QAF-TRZ** and **STF-TRZ**.

 

Table 2 Electroluminescence characteristics of the devices

| Device | $V^a$ (V) | CE$^b$ (cd A$^{-1}$) | PE$^b$ (lm W$^{-1}$) | EQE$^c$ (%) | CIE$^d$ ($x$,$y$) |
|---|---|---|---|---|---|
| **B1** | 3.4 | 45.0 | 47.8 | 19.4/18.3/17.2 | (0.16,0.35) |
| **B2** | 3.5 | 30.8 | 27.5 | 12.7/12.3/11.3 | (0.17,0.37) |
| **G1** | 2.8 | 80.0 | 91.0 | 21.0/20.4/20.0 | (0.34,0.63) |
| **G2** | 2.9 | 72.0 | 76.0 | 19.0/18.9/18.8 | (0.34,0.61) |
| **R1** | 3.8 | 26.5 | 24.1 | 22.6/21.8/17.1 | (0.63,0.36) |
| **R2** | 3.8 | 29.0 | 25.3 | 19.4/19.0/15.5 | (0.62,0.37) |

$^a$ Driving voltage at 100 cd m$^{-2}$. $^b$ Maximum value of current efficiency and power efficiency. $^c$ EQEs of maximum value, 100 cd m$^{-2}$ and 1000 cd m$^{-2}$. $^d$ CIE (Commission International de l'Eclairge); measured at a driving current density at 5 mA cm$^{-2}$.

alignment. The chemical structures of these commercial materials are shown in Fig. S4 (ESI†). We all know that the $E_T$ of the PHOLED host is higher than that of the emitters for effective exciton confinement, better energy transfer from the host to the guest and reducing the non-radiative transition. In this work, the $E_T$ of **QAF-TRZ** and **STF-TRZ** are 2.88 and 2.86 eV, respectively, which indicates that all are appropriate as the host for **FIrpic** ($E_T$ = 2.62 eV). We first fabricated the blue devices by varying the concentration of FIrpic from 10 to 20% (Table S1, ESI†), and the optimized concentration was 15%. The current density–voltage–luminance (*J*–*V*–*L*) characteristics for both **B1** and **B2** are shown in Fig. S5a (ESI†) and their device performance is summarized in Table 2. Device **B1** exhibits a maximum EQE, current efficiency (CE), and power efficiency (PE) of 19.4%, 45 cd A$^{-1}$ and 47.8 lm W$^{-1}$, respectively. The EQE can be maintained as 17.2% at 1000 cd m$^{-2}$. However, device **B2** shows a maximum EQE, CE, and PE of 12.7%, 30.8 cd A$^{-1}$ and 27.5 lm W$^{-1}$, which reveals an apparently lower device performance as compared with **B1** (Fig. 3c). Conventional hosts such as 1,3-bis(*N*-carbazolyl)benzene (mCP) and 2,6-bis(3-(carbazol-9-yl)-phenyl)pyridine (26DCzppy) were also used for comparison. The device results are summarized in Table S2 (ESI†). Among them, **QAF-TRZ** shows the best device performance, making it a good candidate as a host material for PhOLED.

To further investigate the difference in the blue PHOLED performance under the same device structure, we fabricated electron- and hole-only devices (**EOD** and **HOD**) to estimate their charge mobilities. The device structures are as follows: ITO/TmPyPB (20 nm)/**QAF-TRZ** or **STF-TRZ** (100 nm)/TmPyPB (20 nm)/Liq (2 nm)/Al (100 nm) (as **EOD**) and ITO/$MoO_3$ (10 nm)/**QAF-TRZ** or **STF-TRZ** (100 nm)/$MoO_3$ (10 nm)/Al (100 nm) (as **HOD**). As shown in Fig. 3d, the *J*–*V* curves of **QAF-TRZ** and **STF-TRZ** almost overlap under the same driving voltages in the **EOD** device, indicating that the two host materials have similar electron mobility. On the contrary, **QAF-TRZ** shows a higher current density than **STF-TRZ** at a low driving voltage in the **HOD**. Therefore, the better hole mobility of **QAF-TRZ** may favor the hole-electron combination for forming excitons in device **B1**.

Furthermore, green and red PHOLEDs were also fabricated with device structures of ITO/HAT-CN (10 nm)/TAPC (40 nm)/TCTA (10 nm)/**QAF-TRZ** or **STF-TRZ**:**Ir(ppy)$_2$acac** 10 wt% (20 nm)/TmPyPB (45 nm)/Liq (2 nm)/Al (100 nm) and ITO/HAT-CN (10 nm)/TAPC (40 nm)/TCTA (10 nm)/**QAF-TRZ** or **STF-TRZ**:**Ir(MDQ)$_2$acac** 6 wt% (20 nm)/TmPyPB (50 nm)/Liq (2 nm)/Al (100 nm) (**G1**, **R1** for **QAF-TRZ** and **G2**, **R2** for **STF-TRZ**). The $E_T$s of green (**Ir(ppy)$_2$acac**) and red (**Ir(MDQ)$_2$acac**) emitters are 2.4 eV and 2.0 eV, respectively, which are much lower than those of the hosts, and therefore can realize effective energy transfer. The device performance is shown in Fig. 4 and also summarized in Table 2. It can be seen that the maximum EQE, CE, and PE of **R1** and **R2** are 22.6%, 26.5 cd A$^{-1}$, and 24.1 lm W$^{-1}$ and 19.4%, 29.0 cd A$^{-1}$, and 25.3 lm W$^{-1}$, respectively. The EQE of **R1** based on the **QAF-TRZ** is among the highest value in red PHOLEDs. Also, the EQE can be kept as high as 17.1% at 1000 cd m$^{-2}$. Moreover, the green devices (**G1** and **G2**) based on our two host materials exhibit maximum EQE, CE, and PE of 21.0%, 80 cd A$^{-1}$, and 91 lm W$^{-1}$ and 19%, 72 cd A$^{-1}$, and 76 lm W$^{-1}$, respectively. Notably, **G1** and **G2** have quite similar performance and low-efficiency roll-off. At a luminance of 1000 cd m$^{-2}$, the EQE of devices **G1** and **G2** remain 20% and 18.8%, and merely decrease by 4% and 1% from their maximum values, respectively. This low roll-off property is mainly attributed to the well-balanced charge injection and better recombination arisen from the high $E_T$ of the hosts. The *J*–*V*–*L* characteristics of green and red devices are exhibited in Fig. S5b and c (ESI†), respectively. In addition, both hosts almost lead to identical RGB EL emissions (Fig. S5d, ESI†), *i.e.*, 472 nm for **B1** and **B2**, 524 nm for **G1** and **G2**, and 612 nm for **R1** and **R2**. Thus, there

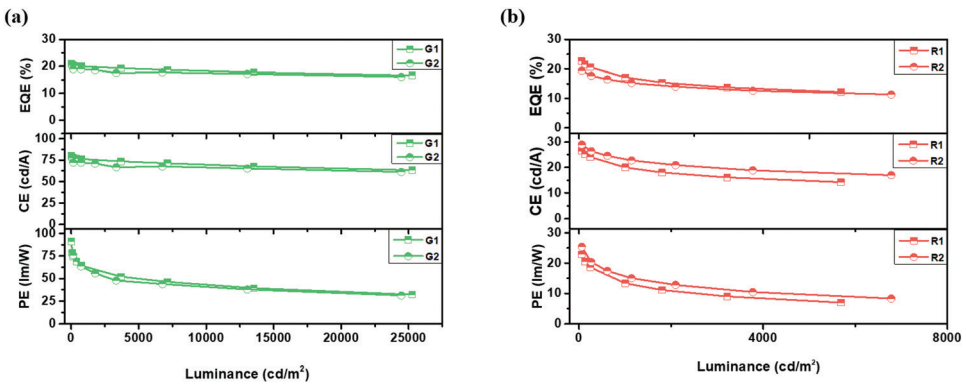


Fig. 4 (a) Green and (b) red PHOLEDs device performance for **QAF-TRZ** and **STF-TRZ**.

is no other emission peak in the EL spectra, substantiating an efficient energy transfer from the hosts to the emitters.

## Conclusion

We have designed and synthesized two host materials, **QAF-TRZ** and **STF-TRZ**, for red, green and blue PHOLEDs. Both materials have excellent thermal properties with a high $T_d$ of over 420 °C. The EQE of the blue PHOLED reached nearly 20% when using **QAF-TRZ** as the host. The maximum EQEs for the green PHOLEDs **QAF-TRZ** and **STF-TRZ** as the hosts were 21% and 19%, respectively. Both the green PHOLEDs exhibited a low-efficiency roll-off, in which the EQEs merely decreased by 4% and 1%, respectively, from their maximum values when the devices were driven to a luminance of 1000 cd $m^{-2}$. Moreover, the red PHOLEDs exhibited maximum EQEs of 22.6% and 19.4% using **QAF-TRZ** and **STF-TRZ** as the hosts, respectively, in which the former has the best EQE among all the red PHOLEDs. The superior device performance is attributed to the new rigidified donor moiety with the spiro motif incorporating triazine (at *para* position) type acceptors. The device based on **QAF-TRZ** exhibits even higher efficiencies because it has a higher hole mobility with better charge recombination. We believe our simple spiro-skeleton strategy can facilitate the development of efficient and stable hosts for RGB-based PHOLEDs.

## Conflicts of interest

There are no conflicts to declare.

## Acknowledgements

We acknowledge financial support from the National Key R&D Program of China (No. 2016YFB0400700), the National Natural Science Foundation of China (No. 51773141, 51873139 and 21572152) and the Natural Science Foundation of Jiangsu Province of China (BK20181442). This project is also funded by Collaborative Innovation Center of Suzhou Nano Science & Technology, the Priority Academic Program Development of Jiangsu Higher Education Institutions (PAPD), the 111 Project of The State Administration of Foreign Experts Affairs of China. We greatly thank Yang-Kun Qu for analyzing the molecular simulations.

## References

1 X.-D. Zhu, Y.-L. Zhang, Y. Yuan, Q. Zheng, Y.-J. Yu, Y. Li, Z.-Q. Jiang and L.-S. Liao, *J. Mater. Chem. C*, 2019, **7**, 6714–6720.
2 S. J. Kim, Y. J. Kim, Y. H. Son, J. A. Hur, H. A. Um, J. Shin, T. W. Lee, M. J. Cho, J. K. Kim and S. Joo, *Chem. Commun.*, 2013, **49**, 6788–6790.
3 M. Hu, Y. Liu, Y. Chen, W. Song, L. Gao, H. Mu, J. Huang and J. Su, *RSC Adv.*, 2017, **7**, 7287–7292.
4 C. W. Tang and S. A. VanSlyke, *Appl. Phys. Lett.*, 1987, **51**, 913–915.
5 W. Jiang, L. Duan, J. Qiao, D. Zhang, G. Dong, L. Wang and Y. Qiu, *J. Mater. Chem.*, 2010, **20**, 6131–6137.
6 L.-S. Cui, S.-B. Ruan, F. Bencheikh, R. Nagata, L. Zhang, K. Inada, H. Nakanotani, L.-S. Liao and C. Adachi, *Nat. Commun.*, 2017, **8**, 1–8.
7 R. K. Konidena, K. H. Lee and J. Y. Lee, *Chem. – Asian J.*, 2019, **14**, 313–321.
8 M. Romain, S. Thiery, A. Shirinskaya, C. Declairieux, D. Tondelier, B. Geffroy, O. Jeannin, J. Rault-Berthelot, R. Métivier and C. Poriel, *Angew. Chem., Int. Ed.*, 2015, **54**, 1176–1180.
9 Y. Zhang, J. Lee and S. R. Forrest, *Nat. Commun.*, 2014, **5**, 1–7.
10 C. Adachi, M. A. Baldo, S. R. Forrest and M. E. Thompson, *Appl. Phys. Lett.*, 2000, **77**, 904–906.
11 S. Ye, Y. Liu, K. Lu, W. Wu, C. Du, Y. Liu, H. Liu, T. Wu and G. Yu, *Adv. Funct. Mater.*, 2010, **20**, 3125–3135.
12 P. Wu, W. Song, Z. Xia, Y. Chen, G. Tian, J. Huang and J. Su, *Dyes Pigm.*, 2019, **162**, 153–159.
13 Q. Dong, F. Tai, H. Lian, Z. Chen, M. Hu, J. Huang and W.-Y. Wong, *Dyes Pigm.*, 2017, **143**, 470–478.
14 M. A. Baldo, D. O'brien, M. Thompson and S. Forrest, *Phys. Rev. B: Condens. Matter Mater. Phys.*, 1999, **60**, 14422.
15 M. A. Baldo, D. O'brien, Y. You, A. Shoustikov, S. Sibley, M. Thompson and S. R. Forrest, *Nature*, 1998, **395**, 151–154.
16 M. H. Tsai, H. W. Lin, H. C. Su, T. H. Ke, C. C. Wu, F. C. Fang, Y. L. Liao, K. T. Wong and C. I. Wu, *Adv. Mater.*, 2006, **18**, 1216–1220.
17 D. Zhang, C. Zhao, Y. Zhang, X. Song, P. Wei, M. Cai and L. Duan, *ACS Appl. Mater. Interfaces*, 2017, **9**, 4769–4777.
18 S.-R. Park, S.-M. Kim, J.-H. Kang, J.-H. Lee and M. C. Suh, *Dyes Pigm.*, 2017, **141**, 217–224.
19 X. Zhan, Z. Wu, Y. Lin, Y. Xie, Q. Peng, Q. Li, D. Ma and Z. Li, *Chem. Sci.*, 2016, **7**, 4355–4363.
20 Z. Hu, W. Fu, L. Yan, J. Miao, H. Yu, Y. He, O. Goto, H. Meng, H. Chen and W. Huang, *Chem. Sci.*, 2016, **7**, 5007–5012.
21 V. Govindan, K.-C. Yang, Y.-S. Fu and C.-G. Wu, *New J. Org. Chem.*, 2018, **42**, 7332–7339.
22 A. Chaskar, H. F. Chen and K. T. Wong, *Adv. Mater.*, 2011, **23**, 3876–3895.
23 K. S. Yook and J. Y. Lee, *Adv. Mater.*, 2012, **24**, 3169–3190.
24 K. S. Yook and J. Y. Lee, *Chem. Rec.*, 2016, **16**, 159–172.
25 T. Chatterjee, W.-Y. Hung, W.-F. Tang, H.-F. Chen and K.-T. Wong, *Org. Electron.*, 2017, **50**, 204–212.
26 S. Kumar, D. Li, Y.-K. Wang, Y. Yuan, A. Khan, Z.-Q. Jiang and L.-S. Liao, *Synth. Metods*, 2019, **254**, 42–48.
27 D. Thirion, J. Rault-Berthelot, L. Vignau and C. Poriel, *Org. Lett.*, 2011, **13**, 4418–4421.
28 Y. Tao, C. Yang and J. Qin, *Chem. Soc. Rev.*, 2011, **40**, 2943–2970.
29 M. Romain, D. Tondelier, J. C. Vanel, B. Geffroy, O. Jeannin, J. Rault-Berthelot, R. Métivier and C. Poriel, *Angew. Chem., Int. Ed.*, 2013, **52**, 14147–14151.

 

30 C. Poriel, N. Cocherel, J. Rault-Berthelot, L. Vignau and O. Jeannin, *Chem. – Eur. J.*, 2011, **17**, 12631–12645.
31 C. Poriel, J. Rault-Berthelot, F. Barriere and A. M. Slawin, *Org. Lett.*, 2008, **10**, 373–376.
32 L. Sicard, C. Quinton, J. D. Peltier, D. Tondelier, B. Geffroy, U. Biapo, R. Métivier, O. Jeannin, J. Rault-Berthelot and C. Poriel, *Chem. – Eur. J.*, 2017, **23**, 7719–7727.
33 J. D. Peltier, B. Heinrich, B. Donnio, O. Jeannin, J. Rault-Berthelot and C. Poriel, *Chem. – Eur. J.*, 2017, **23**, 17290–17303.
34 I. Bulut, P. Chávez, S. Fall, S. Méry, B. Heinrich, J. Rault-Berthelot, C. Poriel, P. Lévêque and N. Leclerc, *RSC Adv.*, 2016, **6**, 25952–25959.
35 C. Poriel, J. J. Liang, J. Rault-Berthelot, F. Barrière, N. Cocherel, A. M. Slawin, D. Horhant, M. Virboul, G. Alcaraz and N. Audebrand, *Chem. – Eur. J.*, 2007, **13**, 10055–10069.
36 F. Moreau, N. Audebrand, C. Poriel, V. Moizan-Baslé and J. Ouvry, *J. Mater. Chem.*, 2011, **21**, 18715–18722.
37 Y. K. Wang, Q. Sun, S. F. Wu, Y. Yuan, Q. Li, Z. Q. Jiang, M. K. Fung and L. S. Liao, *Adv. Funct. Mater.*, 2016, **26**, 7929–7936.
38 A. Khan, Y.-K. Wang, C.-C. Huang, S. Kumar, M.-K. Fung, Z.-Q. Jiang and L.-S. Liao, *Org. Electron.*, 2019, 105520.
39 T. Liu, H. Sun, C. Fan, D. Ma, C. Zhong and C. Yang, *Org. Electron.*, 2014, **15**, 3568–3576.
40 P. J. Stephens, F. J. Devlin, C. F. Chabalowski and M. J. Frish, *J. Phys. Chem.*, 1994, **98**, 11623–11627.
41 L. Tian and F. W. Chen, *J. Comput. Chem.*, 2012, **33**, 580–592.